Wind wave and water level dataset for Hornsund, Svalbard (2013-2021)

Zuzanna M. Swirad[1], Mateusz Moskalik[1], Agnieszka Herman[2]

[1]Institute of Geophysics, Polish Academy of Sciences, Warszawa, Poland
[2]Institute of Oceanology, Polish Academy of Sciences, Sopot, Poland
Correspondence to: Zuzanna M. Swirad (zswirad@igf.edu.pl)

Abstract. Underwater pressure sensors were deployed near-continuously at various locations of the nearshore (8−23 m depth) Hornsund fjord, Svalbard between July 2013 and February 2021. Raw pressure measurements at 1 Hz were used to derive mean water levels, wave spectra and bulk wave parameters for 1024 s bursts at hourly intervals. The procedure included subtracting atmospheric pressure, depth calculation, Fast Fourier Transform, correction for the decrease of the wave orbital motion with depth and adding a high-frequency tail. The dataset adds to the sparse in situ measurements of wind waves and water levels in the Arctic, and can be used e.g. for analysing seasonal wind wave conditions and inter-annual trends, and calibrating/validating wave models.

1 Introduction

In situ wave measurements are critical for understanding wave climate, analysing seasonal and inter-annual trends, and calibrating and validating wave transformation models (e.g. Reistad et al., 2011). Spatial distribution of instruments providing wind wave data is irregular and tends to concentrate in mid- and low-latitude coastal areas (e.g. https://www.ndbc.noaa.gov/; Semedo et al., 2015). In the Arctic, the network of such instruments is particularly sparse. There is a pertinent lack of continuous wave data in the Svalbard archipelago where communities, industry infrastructure, and research stations are located. Continuous wave observations in the coastal Arctic are needed to better understand how i) decreasing sea-ice extent – pan-Arctic annual mean extent decrease of 3.5-4.1% per decade (IPCC, 2019) or 1.5 to 3-fold increase of the length of sea-ice free season along pan-Arctic coasts (Barnhart et al., 2014) between 1979 and 2012, ii) increasing frequency and strength of storms (Francis et al., 2011; Wang et al., 2015; Stopa et al., 2016; Waseda et al., 2018), and, in consequence, iii) higher waves acting on Arctic coasts for longer time periods contribute to coastal flooding and erosion, that can cause infrastructure damage (Forbes, 2011).

Our knowledge of the western Svalbard wave climate comes primarily from global spectral models such as NOAA's WaveWatch III (WW3) hindcast (WW3DG, 2019), ECMWF reanalysis projects ERA-40 (1957-2002; Uppala et al., 2005), ERA-Interim (1979-2019; Dee et al., 2011) and ERA5 (1959-present; Hersbach et al., 2020), or NCEP's Climate Forecast System Reanalysis (CFSR; Saha et al., 2014). Arctic Ocean Wave Analysis and Forecast system (Carrasco et al., 2022) is a shorter duration (since 2017), higher resolution (3 km) model that provides hourly e.g. significant wave height (H_s), peak period (T_p) and peak wave direction (θ_p) using ECMWF's WAM model. The 10 km resolution ERA-40 reanalysis data allowed Semedo et al. (2015) to capture seasonal trends in swell and wind sea and the $\geq$ 10 cm per decade increase in winter H_s over the northern Atlantic. Stopa et al. (2016) used CFSR and altimetry data to calculate an average H_s of 1.5 m (99th percentile of 5-6 m) for the period 1992-2014 west of Svalbard. Wojtysiak et al. (2018) observed up to 1 m H_s difference between winter (higher) and summer (lower) months using WW3 (2005−2015; at 0.5º resolution) and ERA-Interim (1979−2015; at 1º resolution), and found a statistically-significant trend of increasing frequency (2 storms per decade) and total duration (4 days per decade) of storms for the Greenland Sea off south-western Svalbard for the 1979−2015 period, with the typical annual values of 10-40 storms and 20-80 days, respectively.

The large-scale models are good for understanding the general trends in the Arctic/Svalbard area, but provide limited information on local-scale wave parameters in specific fjords and bays (Nederhoff et al., 2022). How the open ocean wave conditions translate into wave conditions in the coastal areas is poorly constrained given complex coastal wind patterns and bottom topography (Semedo et al., 2015). Moreover, the large-scale models over-simplify most aspects of wind wave-sea ice interactions. Most operational models use simple empirical formulae for wave attenuation in sea ice (Barnhart et al., 2014; Zhao et al., 2015; Ardhuin et al., 2016).

Herman et al. (2019) used three nested Simulating Waves Nearshore (SWAN; Booij et al., 1999) models to predict wind wave parameters within bays of Hornsund fjord (~15 m depth) taking eastern Greenland Sea WW3 spectra as boundary conditions. They ran the model for two sea-ice free 4-month periods (August – November 2015 and 2016) finding a good agreement between the modelled and measured significant wave height ($r^2 > 0.9$) and mean absolute wave period ($r^2 = 0.63–0.78$). The study added a considerable detail into wind wave transformation in the nearshore environment of Hornsund by including fjord bathymetry, which allowed resolving depth-induced wave breaking and bottom friction on wind conditions. Notably, the study used a subset of the dataset described in this paper to validate the wave spectral model (Herman et al., 2019).

The model of Herman et al. (2019) tested against buoy data performed well for ice-free conditions only. For a bay of Beaufort Sea, Nederhoff et al. (2022) incorporated sea ice into SWAN model which enabled to reliably describe wave climate in 1979–2019. The need for observational data to validate wave models, especially in periods when the sea ice is present, persists.

We present a 7.5-year (2013-07 to 2021-02) wind wave dataset from Hornsund, southern Svalbard (77°N, 15.5°E). Our goal is to increase observational understanding of Arctic wave conditions by providing a dataset that can be further used to e.g. i) analyse the inter- and intra-annual trends in nearshore wind wave conditions, ii) calibrate and validate wave transformation models, iii) quantify the role of sea ice in wave attenuation, iv) create empirical models of wave run-up on high-latitude beaches, and, v) predict future wind wave conditions.

2 Study area

Hornsund is a ~30 km long fjord of SW Spitsbergen, Svalbard (**Fig. 1a**). It has a ~12 km wide and ~100 m deep opening to the Greenland Sea. The average fjord depth is ~100 m with the deeper (200-250 m) central part (**Fig. 1b**; Herman et al., 2019). The tides are semi-diurnal and the average tidal range is 0.75 m (Kowalik et al., 2015). The circulation is cyclonic (counter-clockwise) with the inflow from SW and outflow to the NW (Jakacki et al., 2017).
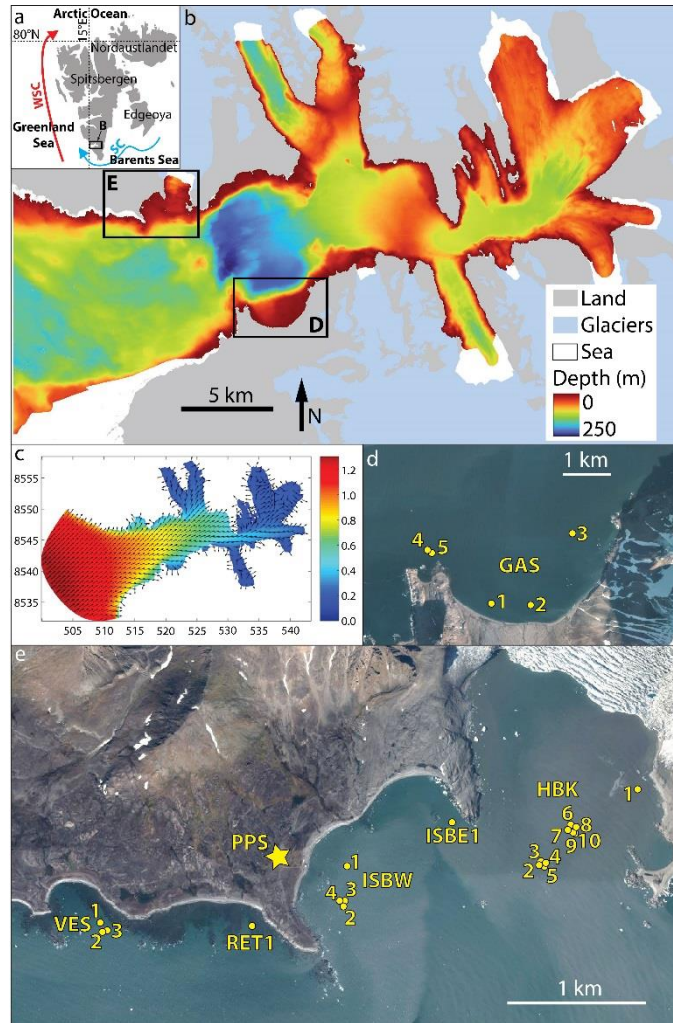
Figure 1: Study area: (a) Svalbard archipelago; WSC = warm West Spitsbergen Current; SC = cold Sørkapp Current; (b) bathymetry of Hornsund fjord (source: Norwegian Hydrographic Service; permit granted to IG PAS); (c) mean significant wave height, H_s (colours, in m) and wind wave direction, θ_p (arrows) from Herman et al. (2019); axis labels refer to Universal Transverse Mercator coordinate system zone 33X (UTM33X) coordinates (in km); location of sensor deployments in southern (d) and northern (e) Hornsund. HBK = Hansbukta, ISB = Isbjørnhamna (W = western, E = eastern), RET = Rettkvalbogen, GAS = Gåshamna, VES = Veslebogen, PPS = Polish Polar Station. Background image © Norwegian Polar Institute (permit granted).

In 1979−2018 easterly winds dominated at the Polish Polar Station (12 m a.s.l.; PPS in **Fig. 1e**) with the mean direction of 124º (annual mean range of 102-140º). Mean wind speed at ~20 m a.s.l. was 5.5 m s^{-1} (Wawrzyniak and Osuch, 2020).

Wave conditions in Hornsund are usually related to the long oceanic swell or mixed swell/wind sea from S−SW with short wind waves formed locally due to predominantly easterly winds. The mean H_s at the fjord mouth is 1.2−1.3 m decreasing to 0.5−0.9 m in the central and to < 0.4 m in the inner parts of Hornsund (**Fig. 1c**). Northern shores of the fjord receive more wave energy than southern shores (Herman et al., 2019).

Hornsund bays (in this study Hansbukta, Isbjørnhamna, Rettkvalbogen, Veslebogen and Gåshamna) have complex shapes and bottom topography with ubiquitous skerries causing strong wave transformation due to refraction and dissipation (Herman et al., 2019).

Sea ice forms locally in the fjord or drifts from the open Greenland Sea. The latter originates east of Svalbard, drifts past the

southern tip of Spitsbergen (Sørkapp) and then northwards along the western Spitsbergen coast with cold Sørkapp Current (blue arrow in **Fig. 1a**). Fast ice (i.e. sea ice attached to the shore) persists during winter months. Muckenhuber et al. (2016)

95 observed a decrease in sea ice (both drift and fast ice) duration and extent between 2000 and 2014. In summer months glacier ice from calving tide-water glaciers (Błaszczyk et al., 2019) may accumulate in bays. Increased storminess coincident with positive air temperature anomalies and the lack of sea ice, in particular in October–December, may contribute to coastal erosion (Zagórski et al., 2015).

3 Methods

100 **3.1 Input data**

Pressure data were collected between 2013-07-21 and 2021-02-12 using RBR virtuoso P (continuous sampling at 4 or 6 Hz interval), RBR duo TD (continuous sampling at 1 Hz interval) and RBR virtuoso wave (1024 s bursts at 30 min interval with 1 Hz sampling interval or at 60 min interval with 2 Hz sampling interval). There were 24 single deployments with duration of 13–599 days (**Table 1**; **Fig. 2**). Initially the deployments were short (< 100 days) and usually restricted to the fieldwork season

105 (late spring to autumn). Since 2015, however, deployments were typically ~1-year long with instrument recovery and re-deployment during summer field campaigns. As a result of the COVID-19 pandemics, it was impossible to recover instruments in summer 2020, and the last two deployments (GAS5 and VES3) were > 550 days long and ended with the battery death.

The instruments were anchored to the sea bed in various locations in northern (Hansbukta, western and eastern Isbjørnhamna,

110 Rettkvalbogen, Veslebogen) and southern (Gåshamna) Hornsund (**Fig. 1d,e**). The raw pressure data are part of the LONGHORN oceanographic monitoring of IG PAS and are provided in Swirad et al. (2022).

Table 1: Details of the pressure sensor deployments for in situ wave measurements in Hornsund, Svalbard. Deployment ID (DepID) refers to bays: HBK = Hansbukta, ISB = Isbjørnhamna (W = western, E = eastern), RET = Rettkvalbogen, GAS = Gåshamna, VES = Veslebogen. LONGHORN ID refers to the IG PAS oceanographic monitoring (Swirad et al., 2022).

DepID	LONGHORN ID	Start	End	Length (days)	Latitude (°N)	Longitude (°E)	Depth (m)	Instrument, serial number
HBK1	P01	2013-07-21	2013-08-10	21	77.0068	15.6509	8	RBR virtuoso P, 52915
HBK2	P02	2013-09-05	2013-12-07	94	77.0010	15.6243	23	RBR virtuoso P, 52915
HBK3	P03	2014-02-01	2014-05-05	94	77.0010	15.6243	23	RBR virtuoso P, 52916
HBK4	P04	2014-06-01	2014-09-02	94	77.0009	15.6245	23	RBR virtuoso P, 52915
HBK5	P05	2014-08-25	2014-11-26	94	77.0009	15.6245	23	RBR virtuoso P, 52916
HBK6	Wave01	2015-06-10	2016-06-02	359	77.0031	15.6298	22	RBR virtuoso wave, 52980
HBK7	Wave04	2016-07-01	2017-05-21	325	77.0031	15.6293	22	RBR virtuoso wave, 52980
HBK8	Wave08	2017-06-09	2018-05-24	350	77.0030	15.6316	22	RBR virtuoso wave, 55113
HBK9	TD01	2018-06-05	2019-01-15	225	77.0029	15.6311	22	RBR duo TD, 82445
HBK10	TD02	2018-12-10	2019-06-09	182	77.0029	15.6311	22	RBR duo TD, 82446
ISBW1	P06	2015-05-26	2015-06-07	13	77.0003	15.5628	9	RBR virtuoso P, 52916
ISBW2	Wave02	2015-06-04	2016-06-03	366	76.9974	15.5608	10	RBR virtuoso wave, 55112
ISBW3	Wave05	2016-06-13	2017-05-23	345	76.9977	15.5605	10	RBR virtuoso wave, 55112
ISBW4	Wave07	2017-06-03	2018-05-22	354	76.9977	15.5599	10	RBR virtuoso wave, 55112
ISBE1	Wave03	2015-06-04	2016-06-03	366	77.0044	15.5935	10	RBR virtuoso wave, 55112
RET1	P07	2015-07-13	2015-07-25	13	76.9943	15.5308	11	RBR virtuoso P, 52915
GAS1	P08	2015-07-13	2015-07-25	13	76.9418	15.8117	8	RBR virtuoso P, 52916
GAS2	P09	2015-08-16	2015-09-09	25	76.9416	15.8482	8	RBR virtuoso P, 52915
GAS3	Wave06	2016-06-17	2017-06-02	351	76.9540	15.8850	11	RBR virtuoso wave, 55113
GAS4	Wave10	2018-06-05	2019-06-10	371	76.9506	15.7710	22	RBR virtuoso wave, 55113
GAS5	Wave12	2019-06-26	2021-01-14	569	76.9505	15.7735	23	RBR virtuoso wave, 55113
VES1	P10	2015-08-16	2015-09-13	29	76.9957	15.4876	11	RBR virtuoso P, 52916
VES2	Wave09	2018-06-05	2019-06-09	370	76.9951	15.4881	16	RBR virtuoso wave, 55112
VES3	Wave11	2019-06-25	2021-02-12	599	76.9952	15.4894	16	RBR virtuoso wave, 55112
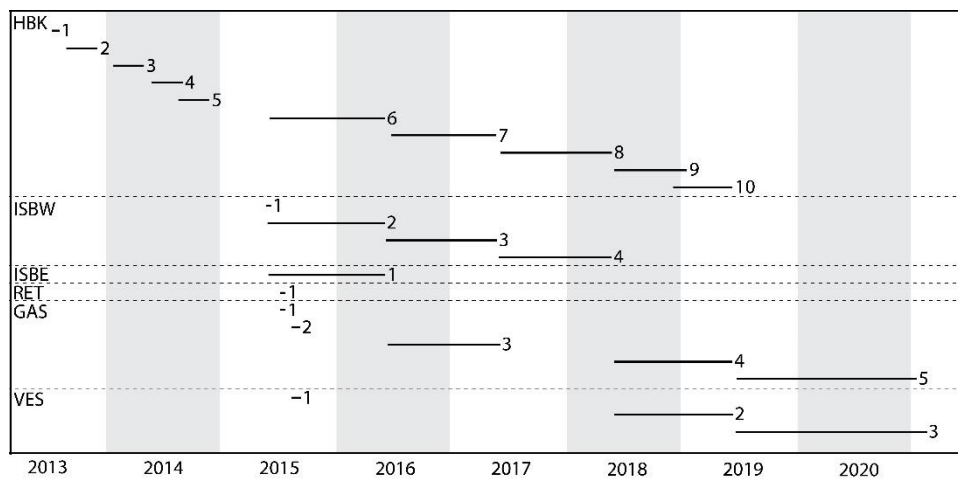
Figure 2: Timespan of pressure sensor deployments for in situ wave measurements in Hornsund, Svalbard. HBK = Hansbukta, ISB = Isbjørnhamna (W = western, E = eastern), RET = Rettkvalbogen, GAS = Gåshamna, VES = Veslebogen.

For consistency the raw data were subsampled to 1024 s bursts at 60 min interval (starting at full hours) with 1 Hz sampling interval. The erroneous bursts at the start and end of deployments were removed. The datasets were cropped to full days so that the first measurement occurs at 00:00:00 UTC (hh:mm:ss) and the last one at 23:17:03 (1024th s after 11pm). These 24
125 deployment files are time series with three columns representing time, burst number and raw pressure in dbar, and are available as part of the dataset (Swirad et al., 2023).

3.2 Burst processing

The deployment files were imported into Spyder (Python 3.9) and processed on the burst-by-burst basis, with an algorithm
130 described below (see also Wang et al., 1986, Karimpour et al., 2017, Marino et al., 2022, and references therein). Importantly, all steps described below are based on the linear wave theory; alternative data processing methods (e.g., Bonneton et al., 2018) might be applied to the original burst data to capture nonlinear effects, but they are not considered here.

Hourly (one per burst) atmospheric pressure P_{air} (mbar) at the sea level was taken from the Polish Polar Station archive
135 (https://monitoring-hornsund.igf.edu.pl/; accessed on 2022-03-28). The water pressure, P_{sea} (dbar) was calculated by subtracting atmospheric pressure from the raw pressure, P_{raw}:

$$P_{\text{sea}} = P_{\text{raw}} - P_{\text{air}}/100. \tag{1}$$

Depth, z (m) was calculated using UNESCO formula (Fofonoff and Millard, 1983) under assumption of constant water
140 temperature of 0ºC, salinity of 35 PSU and latitude $\varphi = 77$ºN:

$$z = \left[\left(\left((-1.82 \cdot 10^{-15}P_{\text{sea}} + 2.279 \cdot 10^{-10})P_{\text{sea}} - 2.2512 \cdot 10^{-5}\right)P_{\text{sea}} + 9.72659\right)P_{\text{sea}}\right]/g, \tag{2}$$

where g (m·s^{-2}) denotes acceleration due to gravity, computed as:

$$g = 9.780318[1 + (5.2788 \cdot 10^{-3} + 2.36 \cdot 10^{-5}x)x] + 1.092 \cdot 10^{-6}P_{\text{sea}}, \tag{3}$$

and x is given by:

145

$$x = \sin^2(\varphi/57.29578). \tag{4}$$

The slowly-varying component of water depth (due to, e.g., tide and storm surge) was removed by subtracting from z a least-square-fitted 2nd order polynomial trend, z_{lf}, resulting in time series z_{hf} (m), related to depth variability associated with wind waves: $z_{\text{hf}} = z - z_{\text{lf}}$. The energy density spectrum at depth z, $E_z(f)$ (in m^2·s), was computed by applying Fast Fourier
150 Transform (FFT; Frigo and Johnson, 2005) to the time series z_{hf}. As already mentioned, the data length used for FFT input was 1024. The Python fft function with default settings was used to compute the spectra, and no windowing was applied.

Finally, the spectrum at the sea surface, $E_0(f)$, was computed from $E_z(f)$ by applying a correction factor $A(f)$ accounting for the decrease of the wave orbital motion (and thus pressure fluctuations) with depth (compare red and blue spectra in **Fig. 3**):
155

$$E_0(f) = E_z(f)/A(f). \tag{5}$$
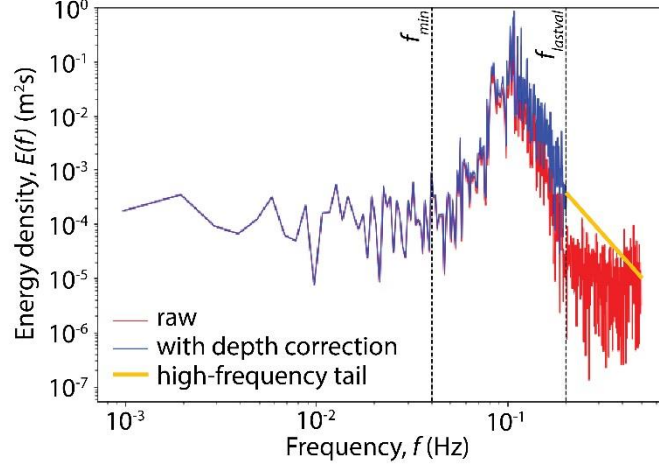
Figure 3: An example of wave energy density spectrum computed with the algorithm described in the text (deployment HBK9 burst #1): raw spectrum $E_z(f)$ at the depth of the logger (red), depth-corrected spectrum $E_0(f)$ (blue), and the analytical high-frequency tail (yellow). Frequency $f_{\min} = 0.04$ Hz is the minimum frequency used to calculate mean wave parameters, and f_{lastval} is the highest frequency reliably measured. The plot is limited to $f = 0.5$ Hz which is the upper limit of the observation data. Wave parameters are calculated in two versions, for $f_{\min} < f < f_{\text{lastval}}$ and for $f_{\min} < f < \infty$.

To this end, a set K of basic wavenumber values was defined, $K = \{0, 0.01, 0.02, \cdots, 1000\}$ (m^{-1}), and a corresponding set of basic wave frequencies F, with elements:

$$f_i = \sqrt{gk_i \tanh(k_i h)} / (2\pi), \qquad \text{for each } k_i \in K. \tag{6}$$

The set of correction factors A is then given by:

$$A_i = \cosh\left(k_i(\bar{h} - \overline{z_{\text{lf}}})\right) / \cosh\left(k_i \bar{h}\right), \qquad \text{for each } k_i \in K, \tag{7}$$

where $\bar{h}$ and $\overline{z_{\text{lf}}}$ denote the mean bottom depth and the mean logger depth, respectively (in the present case, with loggers mounted at the bottom, $\bar{h} = \overline{z_{\text{lf}}}$; averaging takes place over burst duration). The correction factor in (5) was calculated by linearly interpolating F and A to the frequencies of the energy spectrum. (Note that g in expression (6) was computed from (3, 4) without the last term in (3), i.e., for $P_{\text{sea}} = 0$.)

As $A(f)$ quickly decreases with increasing wave frequency, the values of $E_0(f)$ computed from (5) become unreliable for f higher than some limiting frequency f_{lastval}. Here, f_{lastval} was computed for each spectrum separately, based on a universal (constant for all spectra) limiting value of A: $A_{\lim} = 0.05$ (note that, consistent with the linear wave theory used throughout this analysis, the values of A depend only on water depth and frequency of a given spectral component, but not on the amplitude of that component). That is, f_{lastval} is the highest frequency for which $A > A_{\lim}$. For all $f > f_{\text{lastval}}$, a high-frequency tail of the form $E_0(f) \sim f^{-4}$ was added after Kaihatu et al. (2007) by extrapolating the trend from the last $n = 10$ reliably estimated $E_0(f)$ values (yellow line in **Fig. 3**):

$$E_0(f) = \tilde{E}_0 f^{-4} \qquad \text{for } f > f_{\text{lastval}}, \tag{8}$$

where:

$$\tilde{E}_0 = \sum_{j=0}^{n-1} E_0\left(f_{\text{lastval}-j}\right) f_{\text{lastval}-j}^{-4} / \sum_{j=0}^{n-1} f_{\text{lastval}-j}^{-8}. \tag{9}$$

3.3 Mean wave parameters

In calculation of mean (integral) wave parameters, frequencies $f < f_\text{min} = 0.04$ Hz (corresponding to wave periods higher than 25 s) were ignored. This limit corresponds to the approximate boundary between wind-generated and infragravity waves, as well as to the lower frequency limit typically used in spectral wave models (e.g., Holthuijsen, 2007). Thus, the mean wave parameters were computed for $f_\text{min} < f < f_\text{max}$. In the final dataset, two sets of those parameters are provided, referred to as observational one (for $f_\text{max} = f_\text{lastval}$) and modelled one (for $f_\text{max} = \infty$). The spectral moments m_n of $E_0(f)$ are defined as:

$$m_n = \int_{f_\text{min}}^{f_\text{lastval}} E_0(f) f^n df + C \frac{1}{3-n} \tilde{E}_0 f_\text{lastval}^{n-3} \qquad \text{for } n \in \mathbb{N}, \qquad (10)$$

where $\tilde{E}_0$ is computed from (9), $C = 0$ if $f_\text{max} = f_\text{lastval}$ and $C = 1$ if $f_\text{max} = \infty$. Based on m_n, the following wave parameters are calculated: the significant wave height H_s, the mean absolute wave period $T_{m0,1}$, the mean absolute zero-crossing period $T_{m0,2}$, and the so-called energy period $T_{m-1,0}$:

$$H_s = 4\sqrt{m_0}, \qquad (11)$$

$$T_{m0,1} = m_0/m_1, \qquad (12)$$

$$T_{m0,2} = \sqrt{m_0/m_2}, \qquad (13)$$

$$T_{m-1,0} = m_{-1}/m_0. \qquad (14)$$

3.4 Output data

There are two output files for each deployment with rows representing bursts. The first one ('DepID_properties.txt') contains the information on burst (number and time), mean water depth $\overline{z_\text{lf}}$, f_lastval, and the four mean wave parameters defined in Eqs. (11–14), in two versions, i.e., for $C = 0$ and $C = 1$, respectively, in formula (10). The second file provides wave energy spectra for frequencies from 0.040039 to 0.5 Hz with step $\Delta f = \frac{1}{1024}$ Hz (472 columns). **Fig. 4** provides a visualisation of an example one-month period of data. **Table 2** provides the dataset content (Swirad et al., 2023).
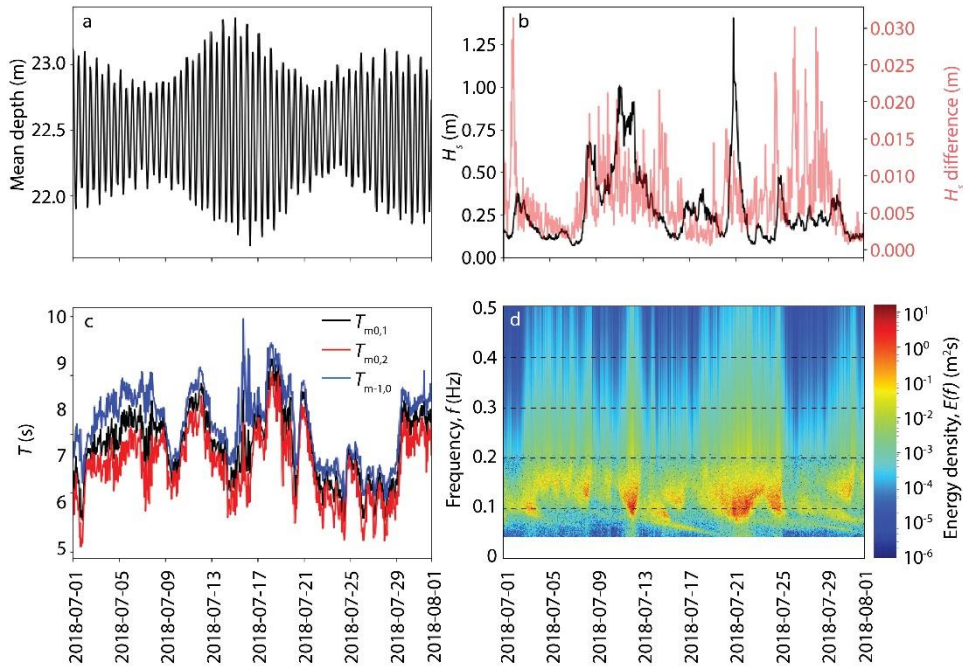
Figure 4: An example of outputs for one month (2018-07) of deployment HBK9: (a) mean depth $\overline{z_{\mathrm{lf}}}$; (b) primary y-axis: significant wave height, H_s for $f_{\max} = \infty$, secondary y-axis: the difference between H_s for $f_{\max} = \infty$ and for $f_{\max} = f_{\mathrm{lastval}}$; (c) wave period, T for $f_{\max} = \infty$, (d) wave energy spectra $E_0(f)$.

Table 2: Dataset content. 'DepID' stands for deployment ID.

File name	Number of files	Type	Rows	Columns
DepID.txt	24	input	Single measurements at 1 Hz frequency (full seconds) in 1024-element bursts (hh:00:00 to hh:17:03) starting at full hours UTC	1. Time ['yyyy-mm-dd hh:mm:ss'] 2. Burst ID [1:n] 3. Measured pressure (dbar)
airpressure.txt	1	input	Hourly measurements starting 2013-07-21 00:00:00 UTC	1. Atmospheric pressure at the sea level (mbar)
bursts2waves.py	1	code	n/a	n/a
DepID_properties.txt	24	output	Single bursts	1. Burst ID [1:n] 2. Time ['yyyy-mm-dd hh:mm:ss'] 3. Mean depth $\overline{z_{lf}}$ (m) 4. $f_{lastval}$ (Hz) 5. H_s (m) for $f_{max} = f_{lastval}$ 6. $T_{m0,1}$ (s) for $f_{max} = f_{lastval}$ 7. $T_{m0,2}$ (s) for $f_{max} = f_{lastval}$ 8. $T_{m-1,0}$ (s) for $f_{max} = f_{lastval}$ 9. H_s (m) for $f_{max} = \infty$ 10. $T_{m0,1}$ (s) for $f_{max} = \infty$ 11. $T_{m0,2}$ (s) for $f_{max} = \infty$ 12. $T_{m-1,0}$ (s) for $f_{max} = \infty$
DepID_spectra.txt	24	output	Single bursts	1-472. Wave energy density, $E(f)$ (m^{2}s) at 0.040039 to 0.5 Hz with 1/1024 Hz step

3.5 Quality control

The instruments remained at the sea bed thanks to the anchor weight. However, a few times they were transported by ice or strong waves resulting in an abrupt change in mean depth visible in the output data (e.g. **Fig. 5a**). This situation occurred three times: in VES1 bursts #83 (depth rise of ~1 m) and #370 (depth drop of ~2.3 m), and in GAS5 burst #13420 (depth rise of ~0.7 m). In the case of VES1 burst #83 and GAS5 burst #13420 it occurred in between bursts with no impact on calculated wave energy spectra and bulk parameters. Therefore, the data are left unchanged. If the dataset is used for tide analysis, timeseries should be split at the depth change event and treated separately. To identify erroneous bursts, we investigated the energy density for $f < 0.5$ Hz and identified two bursts with abnormally high energy density at low frequencies that resulted in erroneous calculation of bulk parameters (e.g. **Fig 5b**): VES1 burst #370 and HBK1 burst #44. In the first case the error resulted from instrument displacement during the burst. In the second case mean depth rised by ~0.5 m, remained higher for a few hours and droped back to a typical level. There was no anomaly in atmospheric pressure and we speculate that the artefact may be due to a presence of glacier ice at the sea surface. In both cases we replaced all output wave parameters with *NaN*.
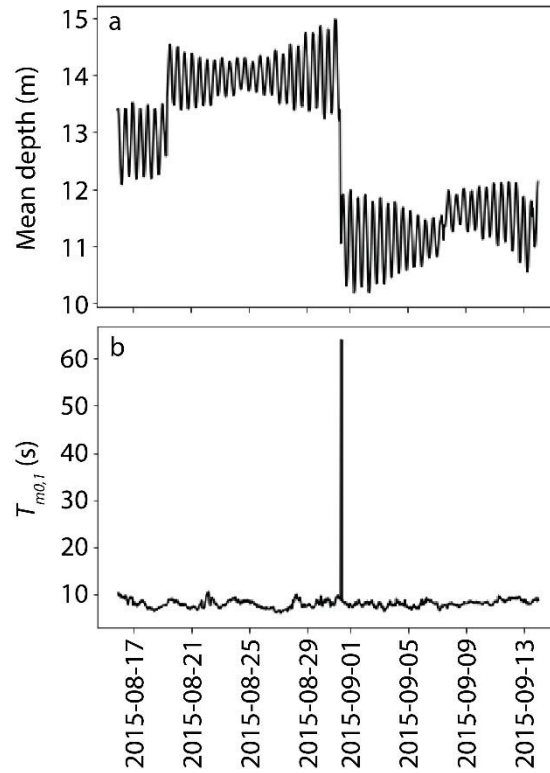
Figure 5: An example of data errors for deployment VES1: (a) mean depth $\overline{z_{\mathrm{lf}}}$; (b) mean wave period $T_{\mathrm{m0,1}}$ for $f < 0.5$ Hz.

4 Results

230 For all bays except Rettkvalbogen timeseries length exceeded one year providing information on seasonal variability in wind wave conditions. The largest waves characterise Veslebogen, a western-most of the analysed northern bays (**Fig. 6**). Mean full dataset H_{s} ranged from 0.25 m in eastern Isbjørnhamna to 0.43 m in Veslebogen and respective 99th percentile H_{s} equalled 1.21 m and 1.96 m. Waves were the highest in the first and last quarter of the year with the highest mean H_{s} of 0.53 m in October-December and 99th percentile H_{s} of 2.32 m in January-March, both in Veslebogen (**Table 3**). A seasonal trend is also
235 clearly visible in **Fig. 7**. Winter months are characterised by generally higher and longer waves, a finding consistent with the multi-decadal wave model reanalysis of Wojtysiak et al. (2018) for open Greenland Sea, west of Hornsund.
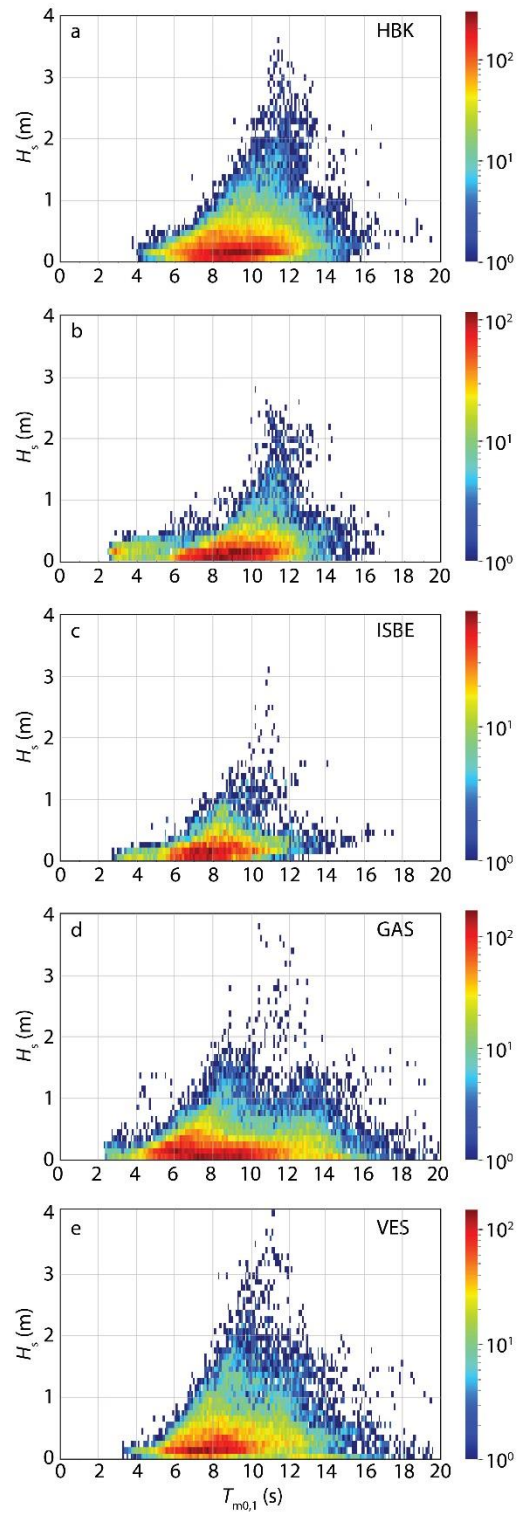
Figure 6: Distribution of significant wave height, H_s (y-axix; range: 0-4 m with 0.1 m bins) and mean absolute wave period, $T_{m0,1}$ (x-axis; range 0-20 s with 0.1 s bins) with $f_{max} = \infty$ for (a) Hansbukta (HBK), (b) western Isbjørnhamna (ISBW), (c) eastern Isbjørnhamna (ISBE), (d) Gåshamna (GAS), and (e) Veslebogen (VES).

Table 3: Summary of significant wave height, H_s: mean, 99th percentile for the full dataset and by quarters of the year, and mean full dataset wave period: mean absolute wave period, $T_{m0,1}$, mean absolute zero-crossing period, $T_{m0,2}$, and energy period, $T_{m-1,0}$. HBK = Hansbukta, ISB = Isbjørnhamna (W = western, E = eastern), GAS = Gåshamna, VES = Veslebogen. Rettkavbogen (RET) is excluded as the 13-day duration is not sufficient to derive seasonal statistics.

	HBK	ISBW	ISBE	GAS	VES
Mean H_s (m)	0.33	0.26	0.25	0.26	0.43
99th percentile H_s (m)	1.71	1.5	1.21	1.33	1.96
Jan-Mar mean H_s (m)	0.44	0.34	0.33	0.35	0.5
Jan-Mar 99th percentile H_s (m)	2.06	1.76	1.5	1.54	2.32
Apr-Jun mean H_s (m)	0.21	0.13	0.16	0.2	0.35
Apr-Jun 99th percentile H_s (m)	0.97	0.48	0.72	1.18	1.71
Jul-Sep mean H_s (m)	0.23	0.16	0.17	0.17	0.35
Jul-Sep 99th percentile H_s (m)	1.03	0.82	1	0.79	1.48
Oct-Dec mean H_s (m)	0.43	0.4	0.35	0.34	0.53
Oct-Dec 99th percentile H_s (m)	1.96	1.91	1.25	1.47	2.25
Mean $T_{m0,1}$ (s)	9.51	9.2	8.31	8.84	9.19
Mean $T_{m0,2}$ (s)	8.72	8.23	7.33	7.93	8.39
Mean $T_{m-1,0}$ (s)	10.36	10.34	9.5	9.93	10.09
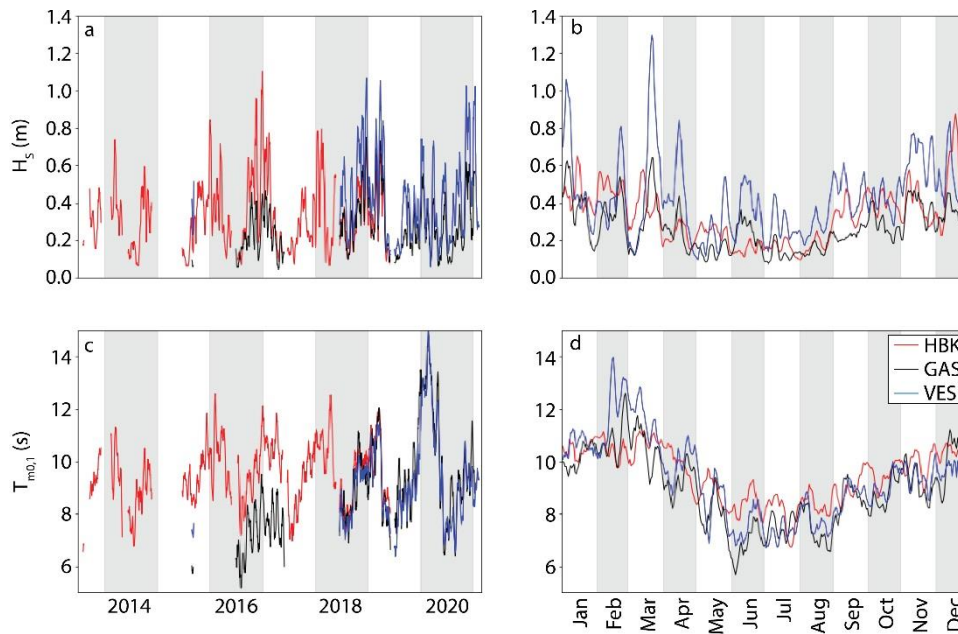
Figure 7: Summary of the wind wave characteristics for Hansbukta (HBK), Gåshamna (GAS) and Veslebogen (VES) for $f_{max} = \infty$: (a) mean daily significant wave height, H_s smoothed with a 15-day moving average; (b) mean daily significant wave height, H_s for days of year smoothed with a 5-day moving average; (c) mean daily absolute wave period, $T_{m0,1}$ smoothed with a 15-day moving average; (d) mean daily absolute wave period, $T_{m0,1}$ for days of year smoothed with a 5-day moving average.

5 Data availability

The inputs, outputs and the Python code described in this manuscript are available in the PANGAEA repository (https://doi.org/10.1594/PANGAEA.954020; Swirad et al., 2023). Raw data downloaded from the instruments are part of the IG PAS LONGHORN oceanographic monitoring and they are available at the IG PAS Data Portal

(https://doi.org/10.25171/InstGeoph_PAS_IGData_NBP_2022_005; Swirad et al., 2022). As the monitoring program is on-going, future raw and processed in the same way data will be uploaded to the IG PAS Data Portal (https://dataportal.igf.edu.pl/).

6 Summary

260 We present the first multi-year continuous wind wave and water level dataset for Hornsund fjord, Svalbard. 24 single deployments of underwater RBR sensors at 8−23 m depth between July 2013 and February 2021 were used to measure water levels in five bays of northern (Hansbukta, western Isbjørnhamna, eastern Isbjørnhamna, Rettkvalbogen, Veslebogen) and one of southern (Gåshamna) Hornsund. Raw data (Swirad et al., 2022) were subsampled to 1024 s sets (~bursts) at 1 Hz measurement interval at 1 h burst interval that were then used to derive mean water levels, wave spectra and bulk wave

265 parameters. We describe the procedure (available also as a Python code) that includes subtracting atmospheric pressure, depth calculation, Fast Fourier Transform, correction for the decrease of the wave orbital motion with depth and adding a high-frequency tail. We performed quality control on the output data. The dataset can be used to e.g. characterise wind wave climate in Hornsund, identify seasonal to inter-annual trends, calibrate and validate wave models (as shown by Herman et al., 2019), and facilitate e.g. analysis of sea ice impact on wave attenuation, empirical modelling of wave run-up on Arctic beaches and

270 predicting future change. We provide individual bursts with pressure times series and the code for the users to apply different analysis methods, use alternative algorithm parameters, analyse nonlinear effects, etc. depending on the application.

Author contributions. MM initiated and maintains the oceanographic monitoring in Hornsund. ZMS secured the funding. ZMS wrote the code and processed the data with the support from AH and MM. All authors wrote the manuscript.

275

Competing interests. The authors declare that they have no conflict of interest.

Acknowledgements. We thank Kacper Wojtysiak for sharing his MATLAB code, Aleksandra Stępień and Adam Słucki (HańczaTECH) for helping in the underwater work, and the Polar Polish Station crew for maintaining the oceanographic and

280 meteorological monitoring. We are grateful to Tsubasa Kodaira and an anonymous reviewer for constructive comments.

Financial support. This study was funded by National Science Centre of Poland (grant no. 2021/40/C/ST10/00146). Acquisition of raw data (Swirad et al., 2022) was funded by National Science Centre of Poland (grant no. 2013/09/B/ST10/04141), IG PAS LONGHORN oceanographic monitoring in collaboration with Polish Polar Station

285 Hornsund, and the Ministry of Education and Science of Poland (statutory activities no. 3841/E-41/S/2022).

References

Ardhuin, F., Sutherland, P., Doble, M., and Wadhams, P.: Ocean waves across the Arctic: attenuation due to dissipation dominates over scattering for periods longer than 19 s: observed ocean wave attenuation across the arctic. Geophys. Res.

290 Lett., 43(11), 5775–5783, https://doi.org/10.1002/2016GL068204, 2016.

Barnhart, K. R., Overeem, I., and Anderson, R. S.: The effect of changing sea ice on the physical vulnerability of Arctic coasts. Cryosphere 8, 1777−1799, https://doi.org/10.5194/tc-8-1777-2014, 2014.

Bonneton, P., Lannes, D., Martins, K, and Michallet, H.: A nonlinear weakly dispersive method for recovering the elevation of irrotational surface waves from pressure measurements. Coastal Engng 138, 1–8,

295 https://doi.org/10.1016/j.coastaleng.2018.04.005, 2018.

Booij, N., Ris, R. C., and Holthuijsen, L. H.: A third-generation wave model for coastal regions. 1. Model description and validation, J. Geophys. Res., 104, 7649–7666, https://doi.org/10.1029/98jc02622, 1999.

Błaszczyk, M., Ignatiuk, D., Uszczyk, A., Cielecka-Nowak, K., Grabiec, M., Jania, J. A., Moskalik, M., and Walczowski, W.: Freshwater input to the Arctic fjord Hornsund (Svalbard). Polar Res., 38, 3506, https://doi.org/10.33265/polar.v38.3506, 2019.

Carrasco, A., Saetra, Ø., Burud, A., Müller, M., and Melsom A.: Product user manual for Arctic Ocean Wave Analysis and Forecasting products ARCTIC_ANALYSIS_FORECAST_WAV_002_014, Issue: 1.6, https://doi.org/10.48670/moi-00002, 2022.

Dee, D. P., Uppala, S. M., Simmons, A. J., Berrisford, P., Poli, P., Kobayashi, S., Andrae, U., Balmaseda, M. A., Balsamo, G., Bauer, P., Bechtold, P., Beljaars, A. C. M., van de Berg, L., Bidlot, J., Bormann, N., Delsol, C., Dragani, R., Fuentes, M., Geer, A. J., Haimberger, L., Healy, S. B., Hersbach, H., Hólm, E. V., Isaksen, L., Kållberg, P., Köhler, M., Matricardi, M., McNally, A. P., Monge-Sanz, B. M., Morcrette, J.-J., Park, B.-K., Peubey, C., de Rosnay, P., Tavolato, C., Thépaut, J.-N., and Vitart, F.: The ERA-Interim reanalysis: configuration and performance of the data assimilation system. Q. J. R. Meteorol. Soc., 137(656), 553–597, https://doi.org/10.1002/qj.828, 2011.

Fofonoff, N. P. and Millard Jr. R. C.: Algorithms for computation of fundamental properties of seawater. UNESCO Technical Papers in Marine Science, 44, https://darchive.mblwhoilibrary.org/bitstream/handle/1912/2470/059832eb.pdf (accessed 28-11-2022), 1983.

Forbes, D.: State of the Arctic Coast 2010 – Scientific Review and Outlook. Tech. Rep., International Arctic Science Committee, Land-ocean Interactions in the Coastal Zone, Arctic Monitoring and Assessment Programme, International Permafrost Association, Helmholtz- Zentrum, Geesthacht, Germany, 178 pp., http://arcticcoasts.org (accessed 28-11-2022), 2011.

Francis, O. P., Panteleev, G. G., and Atkinson, D. E.: Ocean wave conditions in the Chukchi Sea from satellite and in situ observations. Geophys. Res. Lett., 38, L24610, https://doi.org/10.1029/2011GL049839, 2011.

Frigo, M. and Johnson, S. G.: The Design and Implementation of FFTW3. Proc. of the IEEE, 93(2), 216–231, https://doi.org/10.1109/JPROC.2004.840301, 2005.

Herman, A., Wojtysiak, K., and Moskalik, M.: Wind wave variability in Hornsund fjord, west Spitsbergen. Estuar. Coast. Shelf Sci., 217, 96–109, https://doi.org/10.1016/j.ecss.2018.11.001, 2019.

Hersbach, H., Bell, B., Berrisford, P., Hirahara, S., Horányi, A., Muñoz-Sabater, J., Nicolas, J., Peubey, C., Radu, R., Schepers, D., Simmons, A., Soci, C., Abdalla, S., Abellan, X., Balsamo, G., Bechtold, P., Biavati, G., Bidlot, J., Bonavita, M., De Chiara, G., Dahlgren, P., Dee, D., Diamantakis, M., Dragani, R., Flemming, J., Forbes, R., Fuentes, M., Geer, A., Haimberger, L., Healy, S., Hogan, R. J., Hólm, E., Janisková, M., Keeley, S., Laloyaux, P., Lopez, P., Lupu, C., Radnoti, G., de Rosnay, P., Rozum, I., Vamborg, F., Villaume, S., and Thépaut, J. N.: The ERA5 global reanalysis. Q. J. Roy. Meteor. Soc., 1–51, https://doi.org/10.1002/qj.3803, 2020.

Holthuijsen, L.: Waves in Oceanic and Coastal Waters. Cambridge University Press, 387 pp., https://doi.org/10.1017/CBO9780511618536, 2007.

International Panel on Climate Change (IPCC): The Ocean and Cryosphere in a Changing Climate, https://www.ipcc.ch/srocc/home (accessed 28-11-2022), 2019.

Jakacki, J., Przyborska, A., Kosecki, S., Sundfjord, A., and Albretsen, J.: Modelling of the Svalbard fjord Hornsund. Oceanologia, 59, 473–495, https://doi.org/10.1016/j.oceano.2017.04.004, 2017.

Kaihatu, J., Veeramony, J., Edwards, K., and Kirby, J.: Asymptotic behaviour of frequency and wave number spectra of nearshore shoaling and breaking waves. J. Geophys. Res., 112, C06016, https://doi.org/10.1029/2006JC003817, 2007.

Karimpour, A. and Chen, Q.: Wind wave analysis in depth limited water using OCEANLYZ, A MATLAB toolbox. Computers and Geosciences 106, 181–189, https://doi.org/10.1016/j.cageo.2017.06.010, 2017.

Kowalik, Z., Marchenko, A., Brazhnikov, D., and Marchenko, N.: Tidal currents in the western svalbard fjords. Oceanologia, 57, 318–327, https://doi.org/10.1016/j.oceano.2015.06.003, 2015.

Marino, M., Rabionet, I.C., and Musumeci, R.E.: Measuring free surface elevation of shoaling waves with pressure transducers. Continental Shelf Res. 245, 104803, https://doi.org/10.1016/j.csr.2022.104803, 2022.

Muckenhuber, S., Nilsen, F., Korosov, A., and Sandven, S.: Sea ice cover in Isfjorden and Hornsund, Svalbard (2000–2014) from remote sensing data. Cryosphere, 10, 149–158, https://doi.org/10.5194/tc-10-149-2016, 2016.

Nederhoff, K., Erikson, L., Engelstad, A., Bieniek, P., and Kasper, J.: The effect of changing sea ice on wave climate trends along Alaska's central Beaufort Sea coast. Cryosphere, 16, 1609–1629, https://doi.org/10.5194/tc-16-1609-2022, 2022.

Reistad, M., Breivik, Ø., Haakenstad, H., Aarnes, O. J., Furevik, B. R., and Bidlot, J.-R.: A high-resolution hindcast of wind and waves for the North Sea, the Norwegian Sea, and the Barents Sea. J. Geophys. Res., 116(C5), C05019, https://doi.org/10.1029/2010JC006402, 2011.

Saha, S., Moorthi, S., Wu, X., Wang, J., Nadiga, S., Tripp, P., Behringer, D., Hou, Y.-T., Chuang, H.-y., Iredell, M., Ek, M., Meng, J., Yang, R., Mendez, M. P., van den Dool, H., Zhang, Q., Wang, W., Chen, M., and Becker, E.: The NCEP Climate Forecast System Version 2. J. Climate, 27, 2185–2208, https://doi.org/10.1175/jcli-d-12-00823.1, 2014.

Semedo, A., Vettor, R., Breivik, Ø., Sterl, A., Reistad, M., Guedes Soares, C., and Lima, D.: The wind sea and swell waves climate in the Nordic seas. Ocean Dyn., 65(2), 223–240, https://doi.org/10.1007/s10236-014-0788-4, 2015.

Stopa, J. E., Ardhuin, F., and Girard-Ardhuin, F.: Wave climate in the Arctic 1992–2014: seasonality and trends. Cryosphere, 10(4), 1605–1629, https://doi.org/10.5194/tc-10-1605-2016, 2016.

Swirad, Z. M., Moskalik, M., and Glowacki, O.: Sea pressure and wave monitoring datasets in Hornsund fjord. IG PAS Data Portal, https://doi.org/10.25171/InstGeoph_PAS_IGData_NBP_2022_005, 2022.

Swirad, Z. M., Moskalik, M., and Herman, A.: In situ wind wave and water level measurements in Hornsund, Svalbard in 2013-2021. PANGAEA, https://doi.org/10.1594/PANGAEA.954020, 2023.

Uppala, S. M., et al.: The ERA40 reanalysis, Q. J. R. Meteorol. Soc., 131, 2961–3012, https://doi.org/10.1256/qj.04.176, 2005.

Wang, X. L., Feng, Y., Swail, V. R., and Cox, A.: Historical changes in the Beaufort–Chukchi–Bering seas surface winds and waves, 1971–2013. J. Clim., 28, 7457–7469, https://doi.org/10.1175/JCLI-D-15-0190.1, 2015.

Wang, H., Lee, D.-Y., and Garcia, A.: Time series surface-wave recovery from pressure gage. Coastal Engng 10, 379–393, https://doi.org/10.1016/0378-3839(86)90022-0, 1986.

Waseda, T., Webb, A., Sato, K., Inoue, J., Kohout, A., Penrose, B., and Penrose, S.: Correlated increase of high ocean waves and winds in the ice-free waters of the Arctic Ocean. Sci. Rep., 8, 4489, https://doi.org/10.1038/s41598-018-22500-9, 2018.

Wawrzyniak, T. and Osuch, M.: A 40-year High Arctic climatological dataset of the Polish Polar Station Hornsund (SW Spitsbergen, Svalbard). Earth Syst. Sci. Data, 12, 805–815, https://doi.org/10.5194/essd-12-805-2020, 2020.

Wojtysiak, K., Herman, A., and Moskalik, M.: Wind wave climate of west Spitsbergen: seasonal variability and extreme events. Oceanologia, 60, 331–343, https://doi.org/10.1016/j.oceano.2018.01.002, 2018.

The WAVEWATCH III R Development Group (WW3DG): User manual and system documentation of WAVEWATCH III R version 6.07. Tech. Note 333, NOAA/NWS/NCEP/MMAB, College Park, MD, USA, 465 pp. + Appendices, https://github.com/NOAA-EMC/WW3/wiki/files/manual.pdf (accessed 28-11-2022), 2019.

Zagórski, P., Rodzik, J., Moskalik, M., Strzelecki, M. C., Lim, M., Błaszczyk, M., Promińska, A., Kruszewski, G., Styszyńska, A., and Malczewski, A.: Multidecadal (1960–2011) shoreline changes in Isbjørnhamna (Hornsund, Svalbard). Pol. Polar Res., 36(4), 369–390, https://doi.org/10.1515/popore-2015-0019, 2015.

Zhao, X., Shen, H. H., and Cheng, S.: Modeling ocean wave propagation under sea ice covers. Acta Mech. Sin. Xuebao, 31(1), 1–15, https://doi.org/10.1007/s10409-015-0017-5, 2015.

380